Int. J. Electrochem. Sci., 14 **(2019)** 9805 – 9814, doi: 10.20964/2019.10.29

International Journal of ELECTROCHEMICAL SCIENCE
www.electrochemsci.org

Co doped MoS_2 as Bifunctional Electrocatalyst for Hydrogen Evolution and Oxygen Reduction Reactions

Congrong Wang[1], Shun Wang[1], Jianguo Lv[1,3,] , Yuxuan Ma[1], Yongqi Wang[1], Gaoliang Zhou[1], Mingsheng Chen[2], Min Zhao[1,3], Xiaoshuang Chen[4,*], Lei Yang[5]*

[1] School of Physics and Materials Engineering, Hefei Normal University, Hefei 230601, China
[2] School of Electronic Information and Electrical Engineering, Hefei Normal University, Hefei 230601, China
[3] Key Laboratory for Photoelectric Detection Science and Technology of Education Department of Anhui Province, Hefei Normal University, Hefei 230601, China
[4] National Laboratory for Infrared Physics, Shanghai Institute of Technical Physics, Chinese Academy of Sciences, Shanghai 200083, China
[5] Department of Chemistry and Materials Engineering, Hefei University, Hefei 230601, China
[*]E–mail: lvjg1@163.com (J. Lv), xschen@mail.sitp.ac.cn (X. Chen).

Received: 25 May 2019 / *Accepted:* 1 August 2019 / *Published:* 30 August 2019

Pure MoS_2 and MoS_2 compounds were doped with Co using a hydrothermal method. XRD results indicate that two of the five diffraction peak results at 9.2° and 18.2° may be attributed to low crystallinity of MoS_2. The (002) diffraction peaks for the Co-doped MoS_2 shifted to smaller angle, which may be due to the Mo^{4+} ions (r =0.65 Å) having been replaced by larger Co^{2+} ions (r =0.74 Å). Raman results show that the intensity of the A_{1g} mode was greater than that of the E^1_{2g} mode for our samples; this indicates that the samples have edge-terminated structures and possess more electrocatalytic active sites. The results of XPS also confirm that the cobalt ions substituted molybdenum atoms into the lattice of MoS_2. Results from the electrocatalytic test confirms that cobalt doping reduces the charge transfer resistance and increases the electrocatalytic active sites, which are conducive to improving its electrocatalytic performance.

Keywords: Co-MoS_2; electrocatalysts; hydrogen evolution reaction; oxygen evolution reaction

1. INTRODUCTION

Many of our current environmental problems are a results of fossil fuel emission, which seriously affect human survival and development. Hydrogen production from water splitting has been regarded as a promising technology capable of meeting the needs of development and overcome the current environmental issues we face [1]. Howeer, it is well known that hydrogen evolution reaction

(HER) requires an efficient catalyst to be effective. The noble metal palladium and other Pt-based materials possess high catalytic activity for HER [2-4], but large-scale applications have been limited by their high cost and scarcity of supply. In the past few years, significant amounts of research have been devoted to develop new and non-noble metal electrocatalysts for HER [5-7]. Various non-noble metal-based electrocatalysts such as carbides, selenide, nitrides, and transition metal sulphides have been adopted as alternative materials for HER, with the transition metal sulphides as the most promising alternative materials. MoS_2, a transition metal sulphide with a two-dimensional layered structure, has a unique grapheme-like structure, providing MoS_2 good electrocatalytic performance and mechanical strength. It is well known that the electrocatalytic active sites in MoS_2 catalysts are seated at the exposed Mo and the unsaturated S atoms on the edges of the molecule [8]. However, electrocatalytic performance of bulk MoS_2 has been hindered due to poor intrinsic conductivity and the fewer electrocatalytic activity edge sites [9]. In order to promote the electrocatalytic performance of MoS_2, a layered structure of MoS_2 was designed and constructed by doping and coupling with other two-dimensional structural materials, which can enhance the conductivity and electrocatalytic activity edge sites of MoS_2 [10-12]. MoS_2 nanosheets were successfully grown on multiwall CNTs using a simple method for enhanced HER performance [13]. The effect of film thicknesses on the HER activity was also investigated using prepared porous 2D MoS_2 films [10]. While the layered structure MoS_2-based nanomaterial is a typical HER electrocatalyst, it is but a good oxygen evolution reaction (OER) electrocatalyst, which is not conducive overall as an applied MoS_2-based electrocatalyst in the general field of water splitting. Bifunctional Co-MoS_2 catalysts involving the HER and OER have seldom been reported in literature [14].

This research report on the results of Co doping for MoS_2 catalysts, which were prepared using a one-step hydrothermal method. The microstructure and morphology were also investigated by means of X-ray diffractometer, Raman spectrometer, and scanning electron microscope, and the chemical compositions and the element valence states of MoS_2 and Co-3-MoS_2 composite were tested using X-ray photoelectron spectroscopy. Finally these results report on the effects of Co doping on the catalytic performance in both acidic and alkaline media with HER and OER reactivity.

2. EXPERIMENTAL

Using a standard preparation process, 4.567g thiourea (CH_4N_2S), and 17.302g hexaammonium heptamolybdate tetrahydrate ($(NH_4)_6Mo_7O_{24}\cdot 4H_2O$) were added to 80 mL deionized water. Then 0.058g, 0.174g, 0.291g, and 0.407g cobalt nitrate ($Co(NO_3)_2$) were dissolved into the mixed solution. The homogeneous solution was obtained by use of magnetic stirring at room temperature. Then the solution was transferred into a 100 mL Teflon-lined autoclave and kept at 220 °C for 24 h in an oven. The autoclave was cooled to room temperature after the reaction. The derived powders were first cleaned ultrasonically several times in absolute ethanol and deionized water, and then dried at 60 °C in a vacuum atmosphere. The Co-MoS_2 prepared from 0.058g, 0.174g, 0.291g, and 0.407g cobalt nitrate were named as Co-1-MoS_2, Co-2-MoS_2, Co-3-MoS_2, and Co-4-MoS_2, respectively. Un-doped molybdenum disulfide was also prepared without nickel nitrate ($Ni(NO_3)_2$) under the same conditions for comparative purposes.

The microstructure of the Co-MoS_2 was investigated by X-ray diffraction analysis (XRD, TD-3500) and Raman spectroscopy (inVia-Reflex, Renishaw). Surface topography of the samples was measured by field emission scanning electron microscopy (FE-SEM, Hitachi S-4800). X-ray photoelectron spectrometer (XPS, Thermo, ESCALAB 250) was used to survey the elemental composition and valence states of the Co-MoS_2 composite. The electrocatalytic performance of the Co-MoS_2 composites were characterized by linear sweep voltammetry (LSV), electrochemical impedance spectroscopy (EIS), and cyclic voltammetry (CV), which were carried out using a CHI 660E electrochemical workstation. Homogeneous catalyst ink was obtained by ultrasonically dispersing 10mg Co-MoS_2 composites in a mixed solution isopropyl alcohol (400 μL) and Nafion solution (5.0%, 25 μL) for 1h. Then, the ink was dripped onto carbon paper (1.0×1.0 cm^2), which was dried at 60 °C for 10 h so as to obtain the working electrode. A pure MoS_2 working electrode was also made using the same process. A carbon cloth and Ag/AgCl (3 M KCl) acted as the counter and reference electrode, respectively.

3. RESULTS AND DISCUSSION

The crystal structures of MoS_2, Co-1-MoS_2, Co-2-MoS_2, Co-3-MoS_2 and Co-4-MoS_2 were characterized using the XRD technique, and the XRD patterns of each sampleare shown in Fig.1. It could be seen from the XRD patterns that the diffraction peaks located at 2θ = 14.3°, 33.5°, and 58.3° correspond to the (002), (101), and (110) crystal face of 2H-MoS_2 with a space group of P63/mmc (JCPDS37-1492). The other two diffraction peaks at 9.2° and 18.2° correspond to the *d* spacings at 9.50 Å and 4.75 Å, which might be attributed to low crystallinity of MoS_2 [15, 16]. The results indicated that a new layered structure with interlayer spacing of 9.5 Å in the sample was greater than that of 6.15 Å in 2H-MoS_2. The strong diffraction peaks at 9.2° clearly demonstrated that the content of layered structure with interlayer spacing of 9.5 Å was more robust than that of 2H-MoS_2. Compared with the pure MoS_2, the (002) diffraction peaks for the Co-doped MoS_2 were shifted at a smaller angle (2θ = 13.82°). These results might be due to the substitution doping of Mo^{4+} ions (*r* =0.65 Å) by Co^{2+} ions (*r* =0.74 Å), which have a larger ionic radius [17].

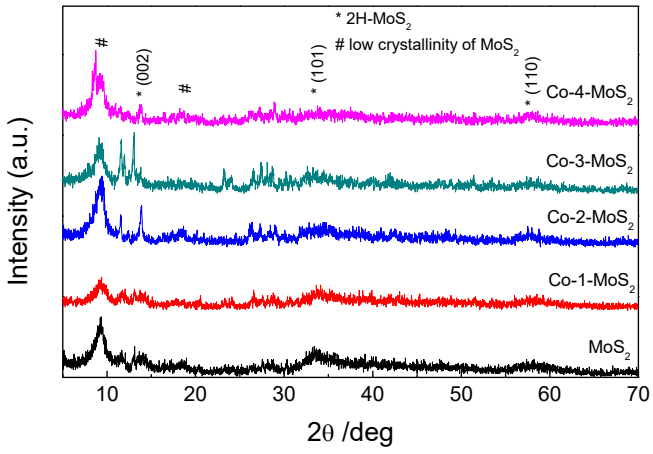

Figure 1. XRD pattern of the Co-doped MoS_2 and pure MoS_2.

Fig. 2 presents the Raman spectra of the samples, which could be used to characterize their microstructure. Two Raman characteristic peaks were located at about 378 and 405 cm^{-1}, which may be indexed to the E^1_{2g} and A_{1g}. corresponding These correspond to the in-plane vibration phonon mode of two S atoms with opposite orientation to Mo atom and the out-of-plane vibration phonon mode of S atoms, respectively [18]. It was reported that the intensity of E^1_{2g} vibration phonon mode and A_{1g} vibration phonon mode were indexed to the edge-terminated and terrace-terminated structures, also respectively [19]. Results showed that the intensity of the A_{1g} mode was greater than that of the E^1_{2g} mode for our samples, indicating that all of the samples present the edge-terminated structures[16, 19], which would offer more edge sites and further improve the activity of electrocatalytic hydrogen production.

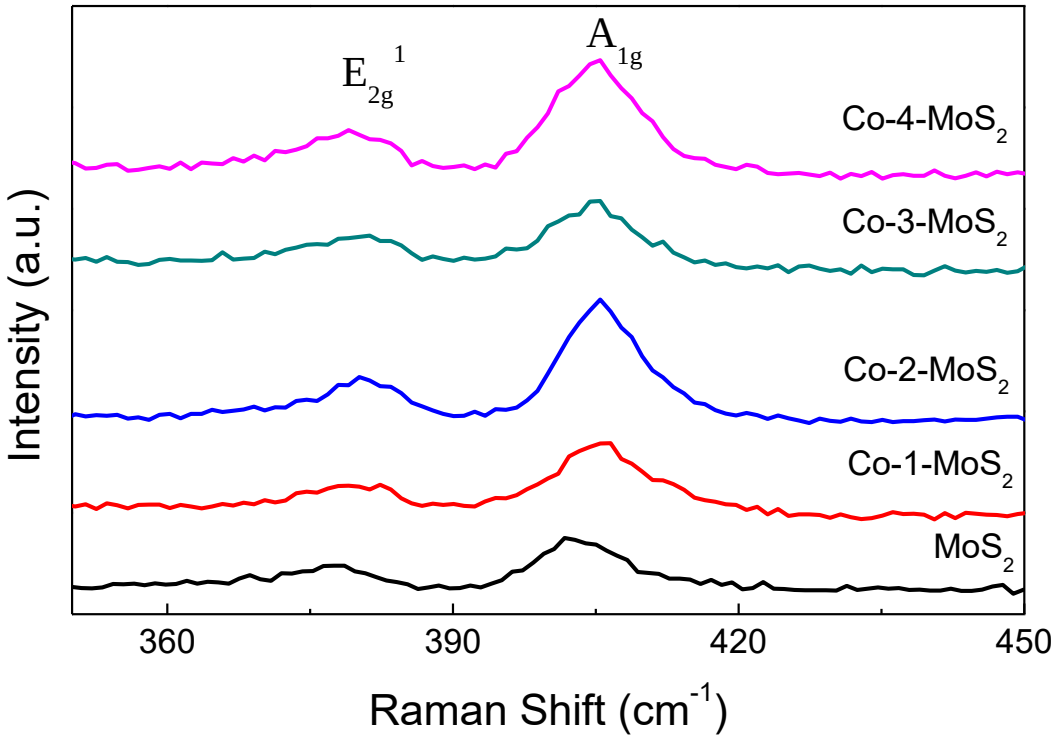

Figure 2. Raman spectra of the Co-doped MoS_2 and pure MoS_2.

Fig.3 visualized the typical FE-SEM images of the pure MoS_2 and Co-MoS_2 nanostructure. A small amount of perpendicularly oriented MoS_2 nanosheets were observed in the pure MoS_2 (in Fig. 3a). Topical flower-like MoS_2 nanosheets were observed in the Co-1-MoS_2 (Fig. 3b). The size of flower shaped MoS_2 nanosheets increases gradually with the increasing amount of Co doping content. The Co-2-MoS_2 and Co-3-MoS_2 exhibit dispersed and homogeneous flower-like nanostructures and have more edge-terminated structures, which might also provide more active for electrocatalytic reactions. However, Co-4-MoS_2 began to lose the perpendicularly oriented feature of MoS_2 nanosheets as the cobalt nitrate increased to 0.407g.

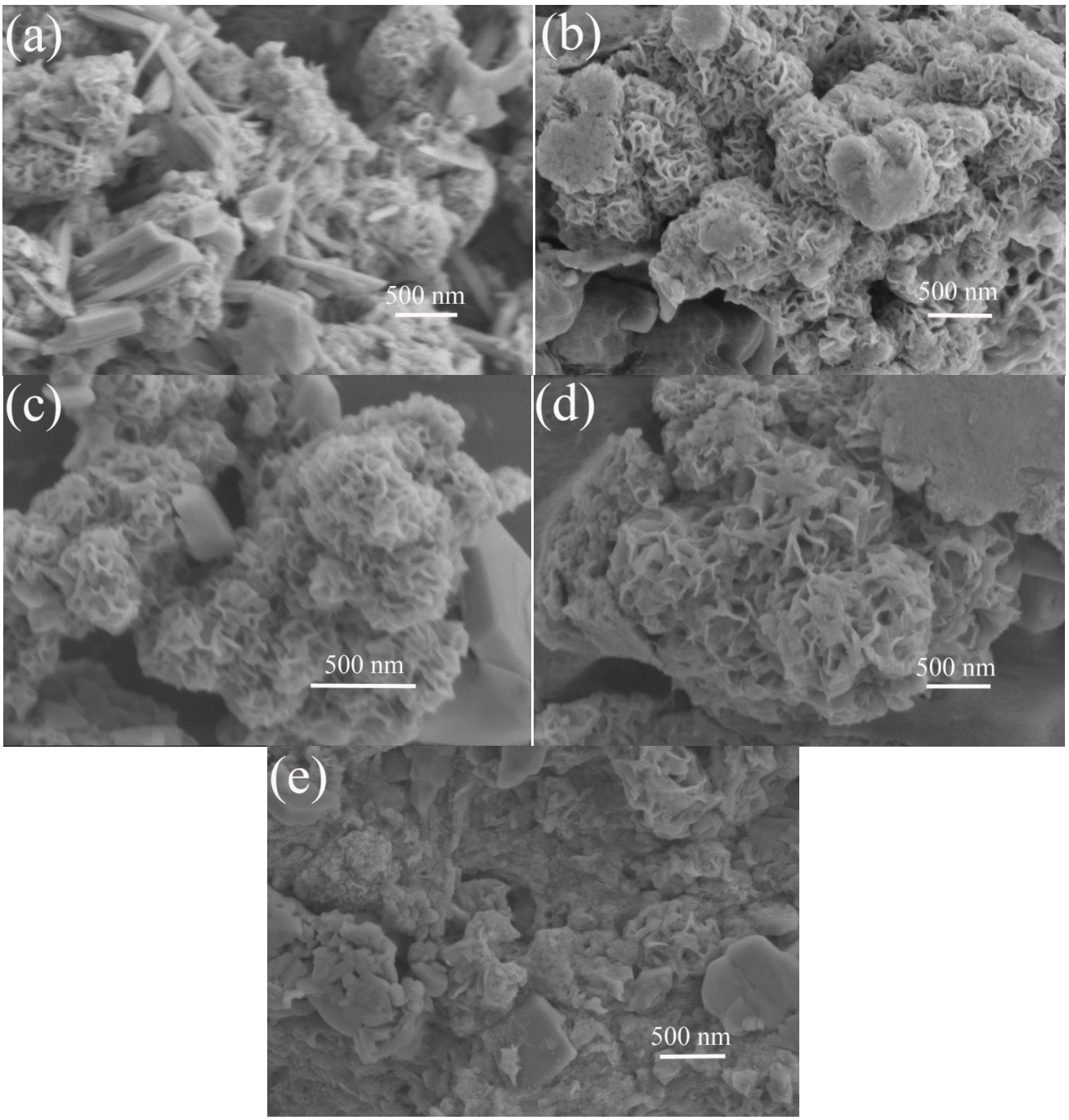

Figure 3. FE-SEM images of (a) pure MoS_2, (b) Co-1-MoS_2, (c) Co-2-MoS_2, (d)Co-3-MoS_2 and (e) Co-4-MoS_2.

XPS has been used to characterize the chemical compositions and the element valence states in the pure MoS_2 and Co-3-MoS_2 composite. The XPS survey spectrum (Fig.4a) showed that the predominant elements were Mo, S, Co, O, and C. The Mo, S and Co elements originated from the Co-3-MoS_2 composite and the C and O elements are most likely present due to the surface adsorption of O_2, H_2O, and CO_2 [20]. The high resolution XPS spectrum of S2p has been presented in the Fig. 4b. The S2p peaks for the Co-3-MoS_2 composite could be divided into five peaks; two peaks were located at ~161.5 and ~162.8 eV were indexed to the S2p3/2 and S2p1/2 orbits from the -2 oxidation state of

the S element, and three peaks were situated at ~164.2 and ~168.8 eV and ~170.1 eV from the C-S and S-O bonds, respectively[21]. The intensity of the three peaks might be improved by the incorporation of Co atoms since it is considered to be an important factor for enhancing the HER activity [22, 23]. Fig. 4c shows the high resolution XPS spectrum of Mo3d. Two strong peaks were located at 228.9 and 231.9 eV and assigned to Mo 3d5/2 and Mo 3d3/2 of Mo(IV), suggesting that Mo(IV) was predominant in the samples. In addition, two weak peaks were seen from Mo 3d5/2 and Mo 3d3/2 of Mo(VI) located at 233.4 and 236.7 eV, indicating that a small amount of the Mo element existed in the form of Mo(VI) compounds. The XPS results indicated that there were Mo(VI) compounds in the Co-3-MoS_2 than in the pure MoS_2. Fig. 4d shows that the Co2p XPS spectrum of Co-3-MoS_2 composite, where the characteristic peaks located at 781.5 eV and 797.7 eV correspond to 2p3/2 and 2p1/2 orbits of Co^{2+}, respectively. The results indicated that the cobalt ions substituted for the molybdenum atoms into the lattice of MoS_2.

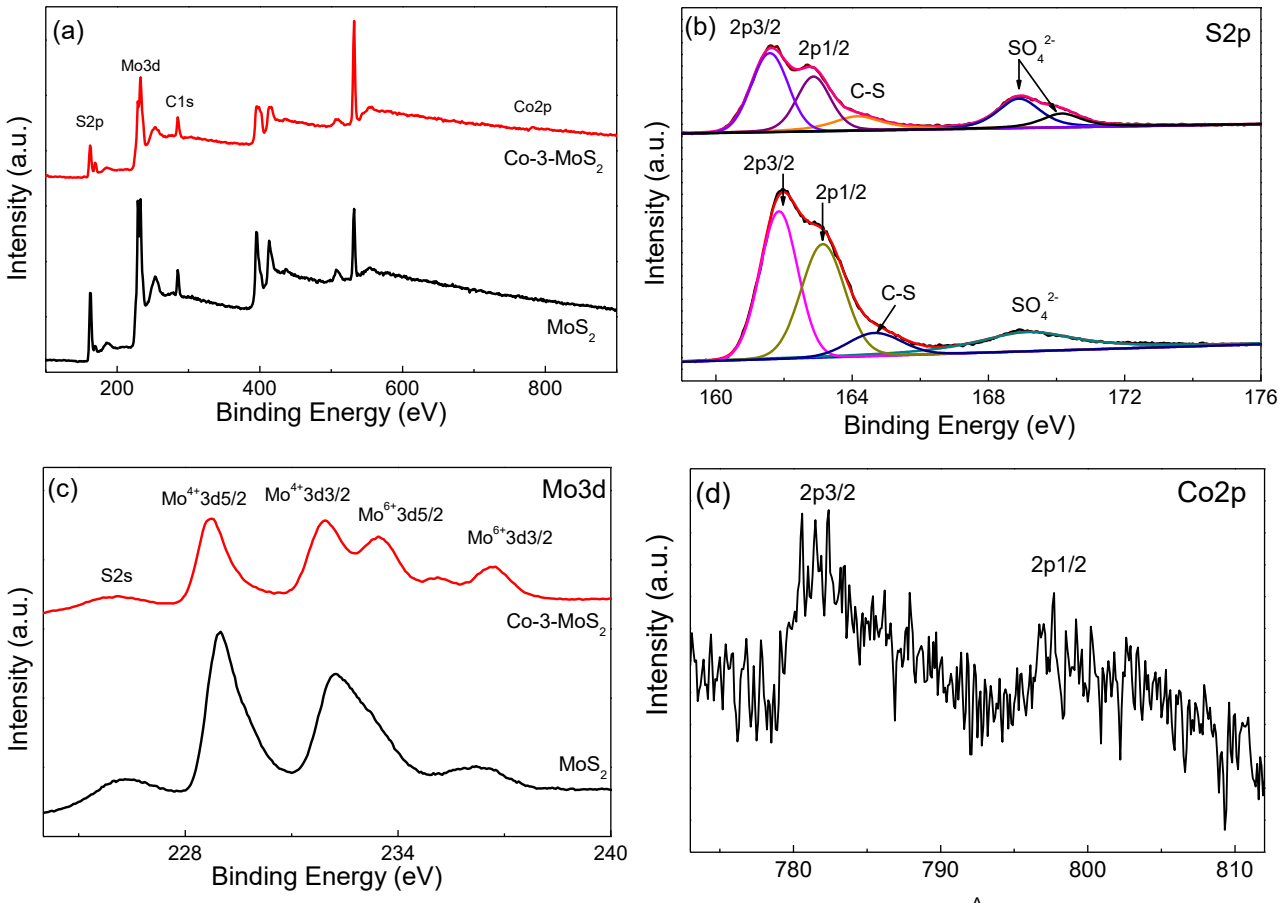

Figure 4. XPS (a)survey spectrum, (b) S 2p, (c) Mo 3d and (d) Co 2p for Co-doped MoS_2 and MoS2.

In order to study the effects of the Co molecule on the HER activities of the Co-MoS_2 composite electrodes, polarization curves of Co-MoS_2 composite electrodes were tested in 0.5M H_2SO_4 solution with a three-electrode system (Fig. 5a). For comparison, the pure MoS_2 and Pt electrodes were also measured using the same method. It can be seen that the Co-3-MoS_2 has the

lowest overpotential of 220 mV (vs. RHE) at 10 mA cm^{-2}, indicating that the Co-3-MoS_2 electrode displays the optimum electrocatalytic activity for HER. The Tafel slope, which is another important parameter for investigating the dynamic process of HER activity, was also used for analysis of the polarization curves. The Tafel curves of pure MoS_2 and Co-MoS_2 composite electrodes, which originated from the LSV polarization curves in the low cathodic overpotential range [24], are displayed in Fig. 5b. The Tafel slope can be calculated by fitting the linear portions of the Tafel curve using the Tafel equation [8, 15]:

$$\eta=a+b\log|j| \quad (1)$$

where η is the overpotential, b is the Tafel slope, and j is the current density. The apparent exchange current density (j_0) can be calculated as follows [8]:

$$j_{0=10}^{-a/b} \quad (2)$$

The obtained Tafel slopes (b) and exchange current density (j_0) of the samples are listed in Table 1. It can be seen that the Tafel slopes of Co-MoS_2 composite electrodes can be reduced by Co doping. The Co-3-MoS_2 composite electrode presents the smallest Tafel slope of 141 mV dec^{-1}, and when compared to other electrodes, the Co-3-MoS_2 composite electrode also has the largest exchange current density of j_0. The smaller Tafel slope implies that there is faster increase of the HER rate as the overpotential increases [24, 25]. The results indicate that Co doping is an effective method for enhancing HER activity.

The electrochemical impedance spectroscopy (EIS) results were used to characterize the electrode kinetics for HER. The impedance spectra of the samples are shown in Fig. 5c and fit using an equivalent circuit model (inset of Fig. 5c). R_s and R_{ct} represent the solution resistance and charge transfer resistance, respectively, where the smaller R_{ct} value reflects the higher HER activity. The fitting R_{ct} values of the samples are listed in Table 1. It can be seen that the Co-3-MoS_2 composite electrode has the smallest semicircle radius in the Nyquist plots, and the R_{ct} of Co-3-MoS_2 composite electrode (~169 Ω) is much smaller than the pure MoS_2 electrode (~6108 Ω). These results indicate that electron transfers are more easily completed in the interface between electrolyte and Co-3-MoS_2 composite electrode [26].

Another important parameter that was explored for the practical application was the durability of catalysts . In order to evaluate the stability of Co-3-MoS_2 composite electrode, polarization curves before and after 1000 cycles were measured; results showed measurements of 0.2 to -0.4 V (*vs.* RHE) with a scan rate of 10 mV s^{-1} (Fig. 5d). It can be seen that the polarization curves after 1000 cycle has a slightly different initial polarization curve in the region of low current density. In addition, the chronoamperometric curve at 248 mV (vs RHE) is present in the inset of Fig. 5d. This result shows that current density of Co-3-MoS_2 composite catalyst decreases slightly, and the Co-3-MoS_2 composite catalyst has steady HER activity for 5 h [27].

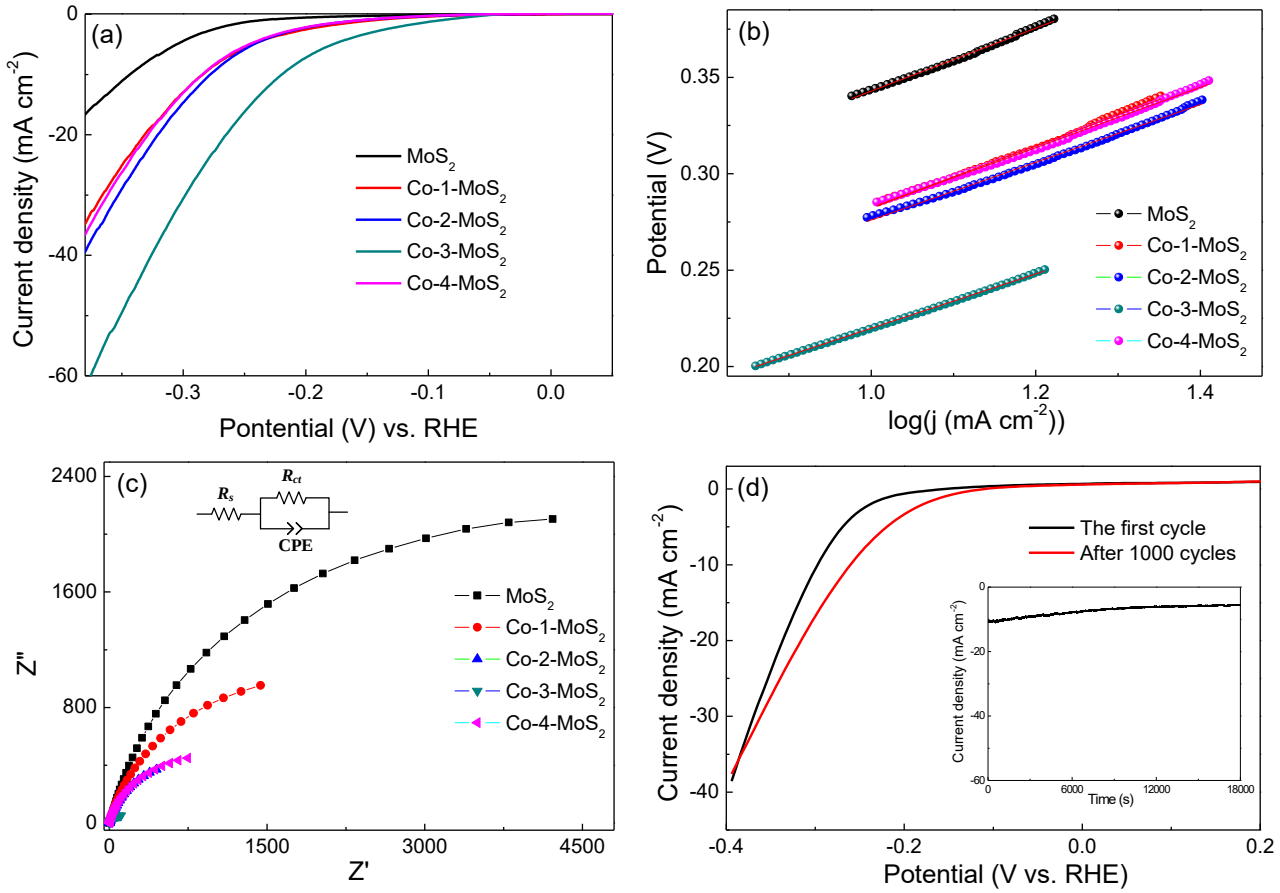

Figure5. (a) HER polarization curves, (b) corresponding Tafel curves, (c) electrochemical impedance spectroscopy of pure MoS_2 and Co-doped MoS_2 in 0.5 M H_2SO_4 (d) HER durability tests for the Co-3-MoS_2.

Table 1. List of the HER catalytic properties of the pure MoS_2 and Co-doped MoS_2 in 0.5 M H_2SO_4

Sample	Potential for 10mA cm^{-2} (mV)	Tafel slope (mV/dec)	j_0 (mA cm^{-2}))	R_{ct} (Ω)	Refs.
MoS_2	343	163.3	0.07965	6108	this work
Co-1-MoS_2	286	160.2	0.17282	2701	this work
Co-2- MoS_2	277	149.8	0.14389	1296	this work
Co-3- MoS_2	220	141.1	0.27655	169	this work
Co-4- MoS_2	286	156.4	0.1567	1308	this work
MoS_2	270	135.0	0.0138	70	22
Ni-MoS_2/Ni foam	207	65	-	-	26
MoS_2@Fe_3O_4	110	52	-	357	28

In this paper, the OER activities of the samples have been measured in the KOH solutions with a concentration of 1.0 M. Fig. 6a shows the LSV plots of MoS_2 and Co-MoS_2 composite electrodes. It can be seen that the Co-2-MoS_2 exhibits the lowest overpotential at 10 mA cm^{-2} of 390 mV (vs. RHE), indicating that the Co-2-MoS_2 electrode has the best OER activity. The results indicate that OER activity of the MoS_2 electrode could be enhanced by moderate Co doping, which could regulate the

electronic structure of MoS_2. The Tafel curves from the LSV curves of the electrode show that the Tafel slope value of the Co-2-MoS_2 electrode is 177 mV dec^{-1} (Fig. 6b), which indicates the it has the optimum OER reaction kinetics [8].

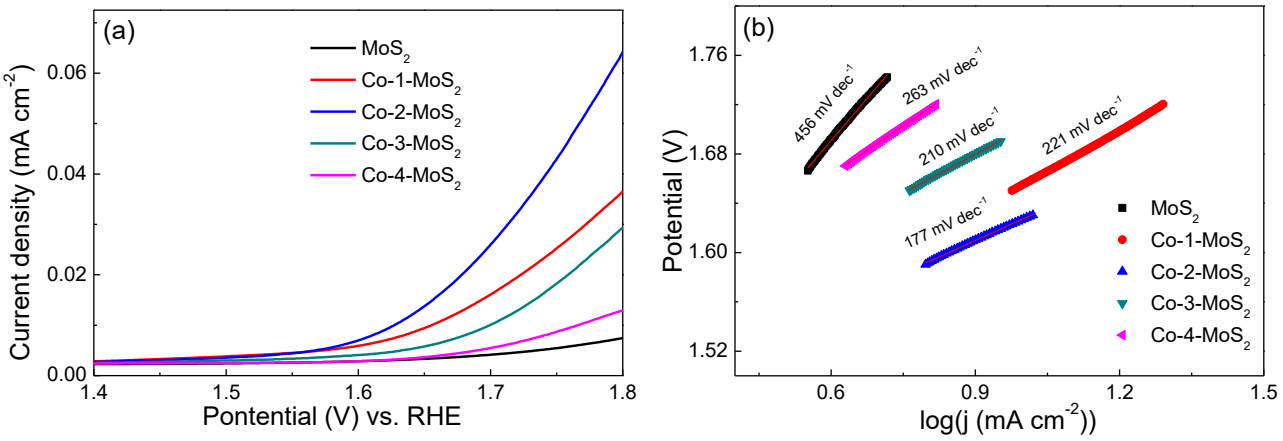

Figure 6. (a) OER polarization curves and (b) Corresponding Tafel curves of pure MoS_2 and Co-doped MoS_2 in 1 M KOH.

4. CONCLUSION

In summary, HER and OER performance of MoS_2-based electrocatalysts have been measured in both acidic and alkaline solutions, respectively. The results show that Co doping could increase the edge-terminated structures and electrocatalytic active sites, as well as reduce the charge transfer resistance, which can be affect electrocatalytic performance. The Co-3-MoS_2 electrocatalyst exhibits the lowest applied potential for HER, the smallest Tafel slope, and good stability. The lowest applied potential for OER and smallest Tafel slop have been observed in the Co-2-MoS_2 electrocatalyst. This study reports a bifunctional Co doped MoS_2 electrocatalyst for HER and OER, which might be a very promising candidate for overall water splitting applications.

ACKNOWLEDGEMENTS
This work was supported by National Natural Science Foundation of China (Nos. 51701001, 61804039), Academic funding projects for Top Talents in Subjects (Majors) of Universities (No. gxbjZD31), Natural Science Foundation of Anhui Higher Education Institution of China (KJ2019A0734, KJ2019A0736, KJ2017A924, KJ2017A002), Natural Science Foundation of Anhui Province (No. 1808085QE126), Doctor Scientific Research Fund of Anhui University (No. J01001927), Youth Core Teacher Fund of Anhui University (No. J01005111) and Foundation of Co-operative Innovation Research Center for Weak Signal-Detecting Materials and Devices Integration Anhui University (No. Y01008411, WRXH201703).

References

1. S.A. Shah, X. Shen, M. Xie, G. Zhu, Z. Ji, H. Zhou, K. Xu, X. Yue, A. Yuan, J. Zhu, Y. Chen, *Small*,

15 (2019) 1804545.
2. M. Pohl, S. Watzele, F. Calle-Vallejo, A. Bandarenka, *ACS Omega*, 2(2017) 8141.
3. W. Xu, X. Zhou, Z. Qi, C. Li, *Research on Chemical Intermediates*, 45 (2019) 1217.
4. R. Solmaz, A. Gündoğdu, A. Döner, G. Kardaş, *International Journal of Hydrogen Energy*, 37 (2012) 8917.
5. T. Hu, K. Bian, G. Tai, T. Zeng, X. Wang, X. Huang, K. Xiong, K. Zhu, *The Journal of Physical Chemistry* C, 120(2016)25843.
6. K.-C. Pham, Y.-H. Chang, D.S. McPhail, C. Mattevi, A.T.S. Wee, D.H.C. Chua, *ACS Applied Materials & Interfaces*, 8 (2016) 5961.
7. Y. Qiu, L. Chai, Y. Su, P. Li, W. Yuan, H. Li, X. Guo, *Dalton Transactions*, 47(2018)6041.
8. L. Xu, S. Wang, *Journal of Electroanalytical Chemistry*, 808 (2018) 173.
9. W.-H. Hu, G.-Q. Han, F.-N. Dai, Y.-R. Liu, X. Shang, B. Dong, Y.-M. Chai, Y.-Q. Liu, C.-G. Liu, *International Journal of Hydrogen Energy*, 41 (2016) 294.
10. M.D. Patel, J. Zhang, J. Park, N. Choudhary, J.M. Tour, W. Choi, *Materials Letters*, 225 (2018) 65.
11. T.-Y. Chen, Y.-H. Chang, C.-L. Hsu, K.-H. Wei, C.-Y. Chiang, L.-J. Li, *International Journal of Hydrogen Energy*, 38 (2013) 12302.
12. X. Chen, K. Zhang, Z. An, L. Wang, Y. Wang, S. Sun, T. Guo, D. Zhang, Z. Xue, X. Zhou, X. Lu, *International Journal of Hydrogen Energy*, 43 (2018) 7326.
13. J. Cao, J. Zhou, Y. Zhang, X. Liu, *Scientific Reports*, 7 (2017) 8825.
14. Q. Xiong, X. Zhang, H. Wang, G. Liu, G. Wang, H. Zhang, H. Zhao, *Chemical Communications*, 54 (2018) 3859.
15. L. Chen, W. Yang, X. Liu, J. Jia, *International Journal of Hydrogen Energy*, 42 (2017) 12246.
16. J. Xie, J. Zhang, S. Li, F. Grote, X. Zhang, H. Zhang, R. Wang, Y. Lei, B. Pan, Y. Xie, *Journal of the American Chemical Society*, 135 (2013) 17881.
17. S. Irfan, S. Rizwan, Y. Shen, L. Li, Asfandiyar, S. Butt, C.-W. Nan, *Scientific Reports*, 7 (2017) 42493.
18. C. Su, J. Xiang, F. Wen, L. Song, C. Mu, D. Xu, C. Hao, Z. Liu, *Electrochimica Acta*, 212 (2016) 941.
19. J. Li, Y. Hou, X. Gao, D. Guan, Y. Xie, J. Chen, C. Yuan, *Nano Energy*, 16 (2015) 10.
20. J. Ma, J. Li, G. Li, Y. Tian, J. Zhang, J. Wu, J. Zheng, H. Zhuang, T. Pan, *Materials Research Bulletin*, 42 (2007) 982.
21. Z.Q. Cao, M.Z. Wu, H.Q. Hu, G.J. Liang, C.Y. Zhi, *NPG Asia Materials*, 10 (2018) 670.
22. L. Wu, X. Xu, Y. Zhao, K. Zhang, Y. Sun, T. Wang, Y. Wang, W. Zhong, Y. Du, *Applied Surface Science*, 425 (2017) 470.
23. D. Wang, X. Zhang, Y. Shen, Z. Wu, *RSC Advances*, 6 (2016) 16656.
24. M. Sheng, W. Weng, Y. Wang, Q. Wu, S. Hou, *Journal of Alloys and Compounds*, 743 (2018) 682-690.
25. Z. He, Y. Huang, F. He, RSC Advances, 6 (2016) 15390.
26. X. Yin, H. Dong, G. Sun, W. Yang, A. Song, Q. Du, L. Su, G. Shao, *International Journal of Hydrogen Energy*, 42 (2017) 11262-11269.
27. Y. Xu, W. Tu, B. Zhang, S. Yin, Y. Huang, M. Kraft, R. Xu, *Advanced Materials*, 29 (2017) 1605957.
28. X. Zhang, P. Ding, Y. Sun, Y. Wang, Y. Wu, J. Guo, *Journal of Alloys and Compounds*, 715 (2017) 53